Monitoring versus prediction of the power of three different PV technologies in the coast of Lima-Peru

Monitoring versus prediction of the power of three different PV technologies in the coast of Lima-Peru

B X Calsi[1], L A Conde[1], J R Angulo[1], J Montes-Romero[2], J A Guerra[1], J de la Casa[2] and J A Töfflinger[1*]

[1]Department of Science, Physics Section, Pontificia Universidad Católica del Perú, Lima, Peru
[2]IDEA Group, Department of Electronics, Universidad de Jaén, Jaén, Spain

*Correspondence: japalominot@pucp.edu.pe

Abstract. This article presents the benefits of two simple analytical models for estimating the outdoor performance of three different photovoltaic technologies in Lima, Peru. The Osterwald and the constant fill factor models are implemented to estimate the maximum power delivered by three photovoltaic module technologies: aluminum back surface field, heterojunction with intrinsic thin-layer and amorphous/microcrystalline thin-film tandem. A 12-months experimental campaign is carried out through measurements of current-voltage curves, irradiance and module temperature. The results show that both models overestimate the modelled power when compared to the measured one. In order to correct the maximum power predicted by both models, a correction factor is introduced. This correction factor allows us to estimate losses and a respective effective nominal power to minimize the prediction error on a monthly and yearly basis. These parameters demonstrate a unique behavior for each technology during different months implying different seasonal impacts of the ambient variables on the module performance. The effectiveness of this correction factor is demonstrated through accuracy measures. It enables the photovoltaic power prediction with an error < 1% for the particular climate in Lima, Peru.

1. Introduction

The growing demand for energy in Peru motivated the government to implement sustainable solutions such as photovoltaic (PV) installations, especially in rural areas, in order to utilize the solar resource in those regions [1–3]. Nevertheless, literature regarding the experimental quantification of PV yield and performance in Peru, even in Lima, is yet scarce due to a limited amount of studies for this region [1,2,4]. Absent knowledge on the performance of PV technologies can lead to technical risks and negative economic impacts in the implementation of PV projects [5].

In order to evaluate the performance of a PV installation, reliable data of the power and its behavior under different meteorological conditions is required. Module manufacturers provide information on the nominal power of the PV modules at standard test conditions (STC). These conditions, defined in standard IEC60904-3 [6], consist of an incident irradiance of 1000 Wm^{-2}, a spectral distribution for air mass (AM) 1.5 and a module temperature of 25 °C. Nevertheless, these conditions are not commonly found under outdoor operation and previous studies indicate that ambient conditions, and thus performance, are site-specific [7–9]. Hence, it becomes evident that on-site studies of different PV module technologies in various regions are required to understand their performance [10].

When such large-scale experimental performance evaluation campaigns are not easily available, the modeling of the PV performance may offer important insights. Several models have been published for estimating the power and energy expected of PV generators [11]. For PV performance prediction purposes, one may often find a trade-off between simplicity and accuracy in those models. In some cases, simplicity may be preferable, particularly if accuracy requires parameters that are not commonly available or use complex algorithms [9]. Studies have been done comparing the accuracy of different models and found that despite the simplicity of some, a high accuracy of the estimated power can be achieved [9,12]. This work aims to determine the goodness of two commonly accepted and simple parametric models for the outdoor performance prediction of three different PV technologies in Lima, Peru.

This paper is organized as follows: section 2 describes the experimental setup, the equipment, and modules considered for this work. section 3 details the applied methodology and the error parameters to determine the goodness of the models. Section 4 presents the results and discussion. Finally, section 5 summarizes the conclusions and future work.

2. Experimental details

The Photovoltaic Research Laboratory is located in the Physics Section of the Pontificia Universidad Católica del Perú (PUCP) (12°4'S, 77°4'W) in Lima. Figure 1 shows the modules under study that are facing north with a tilt angle of 20°. The current-voltage (I-V) tracer is based on a capacitive load and the I-V curve was measured with two Keysight 34465A multimeters. The maximum power is extracted from each I-V curve. A tilted pyranometer EKO MS-80 measured the irradiance at the plane-of-array. Two class B PT100 pasted at the back side of each module were used to measure the module temperature. The full laboratory is described in greater detail in [13,14]; it was developed based on the system described in [15]. The irradiance and module temperature were instantaneously measured at the beginning and the end of the IV curve tracing. The sets of I-V curve data with the meteorological data were recorded every 5 minutes for each PV module.

Figure 1. Photovoltaic Research Laboratory for the monitoring and characterization of PV modules and environmental sensors, localized on the roof-top of the Physics Section at the PUCP.

The experimental campaign was based on three silicon-based PV module technologies: p-type poly-crystalline aluminum-black surface field (Al-BSF), n-type mono-crystalline heterojunction with intrinsic thin-layer (HIT) and amorphous/microcrystalline (a-Si/μc-Si) thin-film tandem. Table 1 shows the characteristic electrical parameters at STC as given by the manufacturer. It also shows the respective calibrated values, which were obtained during the first months of installation [14]. Data sets of the I-V curve, irradiance and module temperature, were collected during one year of monitoring, from June 2019 to May 2020. Each module was cleaned every week to minimize the soiling effects.

Table 1. Characteristic electrical parameters in STC of the PV modules and their calibrated values, taken from [14].

Technology	Electrical parameter	Manufacturer information	Calibrated
Al-BSF	$P_M^*\ (W)$	270	269.2
	$I_{SC}^*\ (A)$	9.32	9.45
	$V_{OC}^*\ (V)$	37.9	37.2
	FF^*	0.76	0.77
HIT	$P_M^*\ (W)$	330	324.6
	$I_{SC}^*\ (A)$	6.07	6.05
	$V_{OC}^*\ (V)$	69.7	70.4
	FF^*	0.78	0.76
a-Si/µc-Si Tandem	$P_M^*\ (W)$	128	127.9
	$I_{SC}^*\ (A)$	3.45	3.32
	$V_{OC}^*\ (V)$	59.8	59.1
	FF^*	0.62	0.65

3. Methodology

In order to maximize the quality of our monitoring data, an effort was made to detect and remove erroneous or inconsistent measurements from the analysis. Firstly, to ensure a constant irradiance during the I-V tracing, the initial and final irradiance were compared. Data sets with a maximum relative difference of 4% with respect to the average value were filtered out [16]. Secondly, the module temperature measurements that widely differed from the calculated nominal operation cell temperature (NOCT) were filtered out [17]. Finally, I-V curves that indicated a shading of the modules in the I-V curve were also removed. Initially, about 121000 measurements were processed by this filtering procedure resulting in a drop of 10%, with about 109000 data sets remaining. These were considered of high quality and used for the current work. The monthly amount of measurements, before and after the filtering procedure for each technology, is presented in Figure 2.

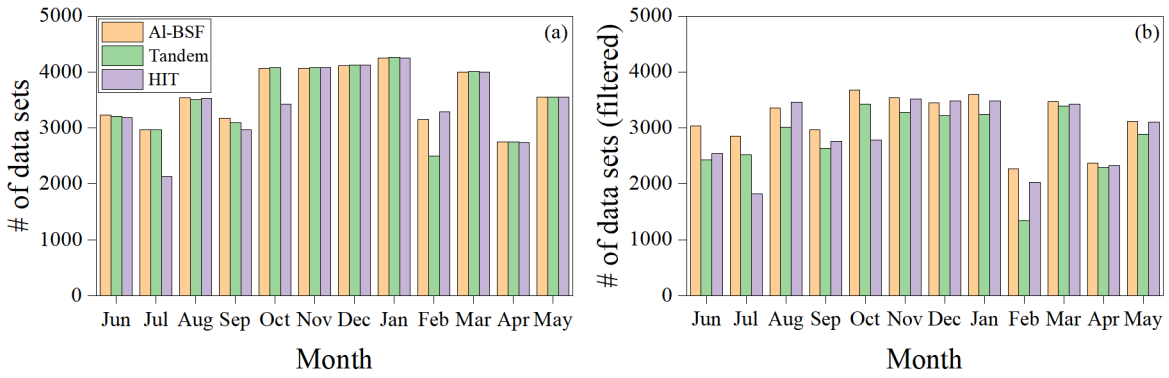

Figure 2. Amount of recorded data sets (a) before and (b) after the filtering procedure for each technology. Obtained from June 2019 to May 2020.

In Figure 3, the classification of local ambient conditions by each season is presented. Spring: September –December, Summer: December-March, Fall: March-June, Winter: June-September. The irradiance and module temperature steps were defined as 50 Wm^{-2} and 5 °C, respectively. For each step, the amount of measurements inside each box was counted and divided by the total amount of measurements of the entire year, represented in % by the colors' scale. The irradiance distribution differs for each season, where high irradiances (from 800 to 1000 Wm^{-2}) appear noticeably in summer season. Nonetheless, a considerable portion of the measurements are taken at low irradiances (from 0 to 300 Wm^{-2}) along the

year, especially in the winter season. Particularly in Lima, cloud presence is predominant during winter, part of spring and autumn [18]. Note that the STC for irradiance (1000 Wm^{-2}) and module temperature (25°C) represented by the black dot, are never met during the entire year. This emphasizes the need to investigate the performance of PV technologies under Lima's climatic condition.

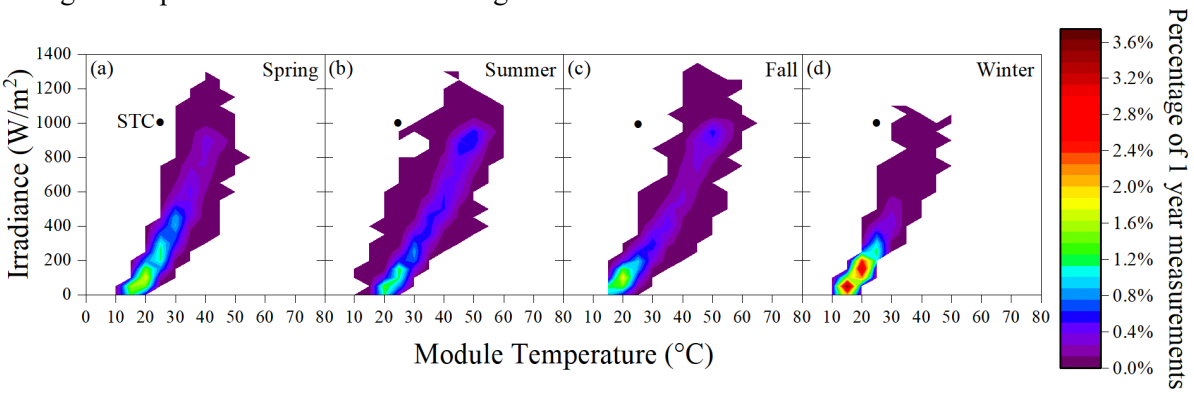

Figure 3. Contour plot indicating the percentage of measurements per range of irradiance and module temperature of the three PV technologies during the different seasons: (a) Spring, (b) Summer, (c) Fall, and (d) Winter.

The models that estimate the maximum power can be classified into two categories: algebraic and numeric. On the one hand, the algebraic models take the entire measured I-V curve and translate it to desired conditions. On the other hand, the numerical models apply semiconductor physics knowledge and estimates the power at the maximum power point (MPP). The latter is computed using analytical methods or solving the implicit equation using numerical iterations. The extend of different methodologies are explained in great detail in [9,11,12]. Two analytical models were selected for the current work, which in prior studies predicted the PV power and energy generation with high accuracy, despite their simplicity [12,19].
The first is Osterwald's model. It is considered one of the simplest and is explained in detail in [20]:

$$P_{Osterwald} = P_M^* \frac{G_i}{G_i^*}[1 + \gamma(T_c - T_c^*)] \quad (1)$$

Where $P_{Osterwald}$ is the predicted maximum power, P_M^* is the nominal power or power delivered by the module at STC, γ ($°C^{-1}$) represents the power temperature coefficient, G_i stands for irradiance, G_i^* is the irradiance at STC (1000 Wm^{-2}), T_c denotes the cell or module temperature, and T_c^* is the cell or module temperature at STC (25 °C).
The second is the constant fill factor (FF_k) model. Which estimates the MPP assuming the fill factor (FF) remains constant through all operation conditions. Additionally, the short-circuit current (I_{SC}) and open-circuit voltage (V_{OC}) have a linear relation with the G_i and T_c, respectively [12,19]:

$$P_{FF_k} = I_{SC}\, V_{OC}\, FF^* \quad (2)$$

$$I_{SC} = I_{SC}^* \frac{G_i}{G_i^*} \quad (3)$$

$$V_{OC} = V_{OC}^*[1 + \beta(T_c - T_c^*)] \quad (4)$$

Where P_{FF_k} is the predicted maximum power, * stands for the corresponding parameter at STC and β ($°C^{-1}$) represents the voltage temperature coefficient.

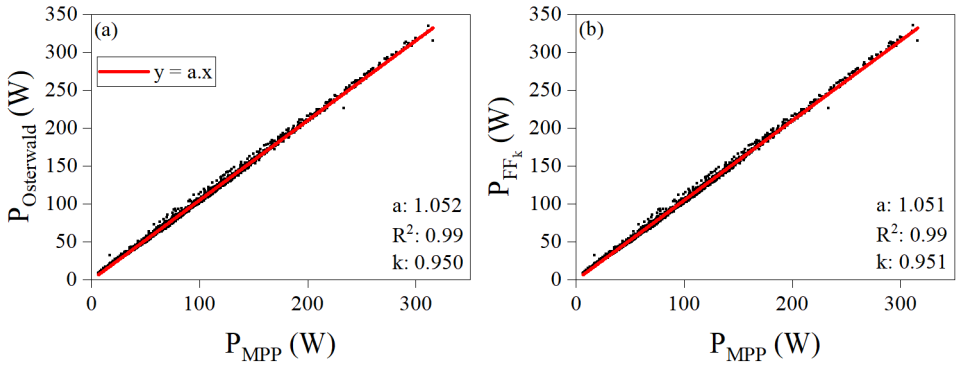

Figure 4. Predicted power by (a) Osterwald ($P_{Osterwald}$) and (b) Constant Fill Factor (P_{FF_k}) models vs. measured maximum power (P_{MPP}) exemplarily for the HIT module in September, 2019.

For each model, the predicted power was calculated using the calibrated parameters in Table 1 and the measured G_i and T_c values. The measured power was obtained from the power at the maximum power point (P_{MPP}) of each I-V curve. Exemplarily, Figure 4 displays the linear relation between the predicted power and the measured P_{MPP} of the HIT module using both models, Osterwald ($P_{Osterwald}$) and P_{FF_k}. Here, the data for the entire month of September 2019 is analyzed. Linear regression was used to correlate the predicted and measured power values. For both cases, the slope a of the linear regression is slightly larger than 1: a = 1.052 and 1.051 for the Osterwald and the FF_k model, respectively. This is an indication that both models are overestimating the power by about 5% for the HIT module for this particular month.

For the correction of the modeled power, a correction factor (k) was introduced. For each lapse of time (month and year), a k is established, this parameter represents the adjustment to the modeled power given the measured power, as seen in equation (5).

$$P_{Ti} = P_{Oi} \cdot k^{-1}, \text{with } k = a^{-1}. \tag{5}$$

Where P_{Oi} represents the instant, maximum power observed by the measurement and P_{Ti} the theoretical power predicted by the model. Values of k higher than 1 represent an underestimation of the power by the model, while lower values than 1 stand for overestimation, and equal to 1 indicates a correct prediction of the measured power, equation (6).

$$k \begin{cases} > 1, & underestimation \\ = 1, & correct\ prediction \\ < 1, & overstimation \end{cases} \tag{6}$$

Furthermore, given the correction factor for each model, a correction of the nominal values can be suggested. In this manner, we propose to define the effective nominal parameters as:

$$P^*_{M,eff} = P^*_M \cdot k_{Osterwald} \tag{7}$$

$$FF^*_{eff} = FF^* \cdot k_{FF_k} \tag{8}$$

Where $k_{Osterwald}$ and k_{FF_k} represent the correction factor for the Osterwald and the FF_k model, respectively. For instance, in figure 4, the resulting values for September 2019 are $k_{Osterwald} = 0.95$

and $k_{FF_k} = 0.951$. $P^*_{M,eff}$ stands for the effective nominal power and FF^*_{eff} for the effective nominal fill factor. By replacing P^*_M with $P^*_{M,eff}$ in equation ((1)) and FF^* with FF^*_{eff} in equation ((2)), we can obtain the "corrected" modeled power.

Two statistical metrics were applied to evaluate the goodness of the afore-mentioned methodology. The normalized root mean square error (NRMSE) provides information on the dispersion of the predicted power with respect to the measured one. Whereas the Normalized Mean Bias Error (NMBE) pictures the deviation or trend of the modeled values:

$$NRMSE = RMSE \cdot [\,\overline{P_O}\,]^{-1}_{year} \cdot 100\% = \left[n^{-1}\sum_{i=1}^{n}|P_{Ti} - P_{Oi}|^2\right]^{1/2} [\,\overline{P_O}\,]^{-1}_{year} \cdot 100\% \quad (9)$$

$$NMBE = MBE \cdot [\,\overline{P_O}\,]^{-1}_{year} \cdot 100\% = \left[n^{-1}\sum_{i=1}^{n}(P_{Ti} - P_{Oi})\right] [\,\overline{P_O}\,]^{-1}_{year} \cdot 100\% \quad (10)$$

Where P_{Ti} and P_{Oi} represent the ith value of the modeled and measured power, respectively, n stands for the number of values considered during the period (month or year). $[\,\overline{P_O}\,]_{year}$ is the yearly average measured maximum power. These definitions of NRMSE and NMBE with reference to $[\,\overline{P_O}\,]_{year}$ differ from the definition used in other works [8,9,12]. In our case, the normalization is made with average power delivered by each technology over the year ($[\,\overline{P_O}\,]_{year}$). This normalization to $[\,\overline{P_O}\,]_{year}$, enables us to compare the NRMSE and NMBE values between months for the three technologies and the methodology [21]. Furthermore, it should be noted that the purpose of the application of the correction factor k is to minimize the NMBE.

4. Results and discussion

Following the procedure mentioned above, the measured and modeled values were compared each month, and the corresponding correction factor was calculated. In Figure 5, the monthly, as well as the yearly correction factor, are depicted for the three PV technologies. For the monthly values, only data from the respective month was evaluated, whereas for the yearly values the entire data of the 12 months was analized.

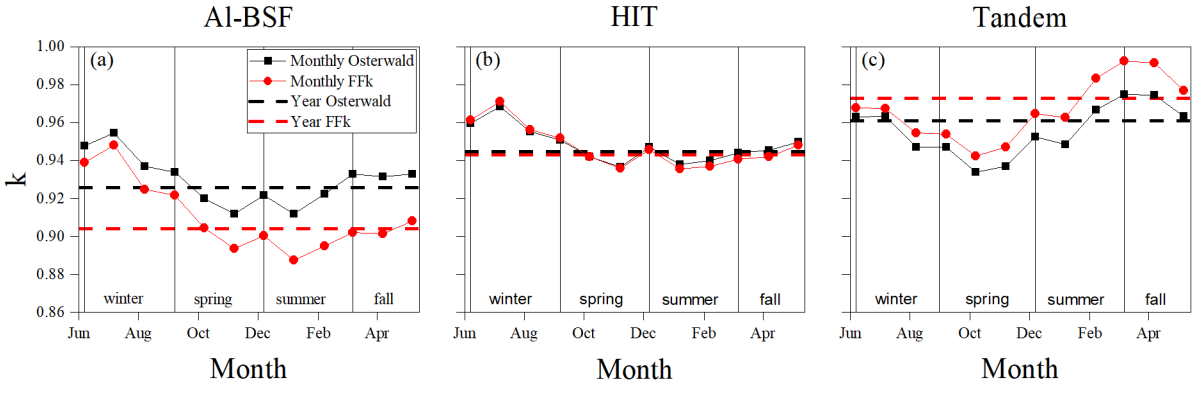

Figure 5. Correction Constant on a monthly and annual basis for both models for three technologies: (a) Al-BSF, (b) HIT, and (c) tandem, from June 2019 – May 2020.

First, it should be noted that the power predicted by both models is overestimated, i.e., $k < 1$, for every technology and for any month. Second, we can observe that the correction factor behaves similarly for both models and all technologies: when the k-value resulting from the Osterwald model increases or decreases from one month to another, so does the one from the FF_k model. This is expected since both

models share similar linear dependencies on the irradiance; see equations (1) to (4). However, the *k*-values of both models can differ depending on the month/season and the technology. For instance, for the Al-BSF technology, Osterwald's model results in a *k* higher than the FF_k model for any month. This means, its predicted power is closer to the experimental power produced by the module. For both models, during spring and summer, the *k* reaches a minimum value and a maximum value during winter. This indicates that both models are most accurate in their maximum power prediction during the winter months. Interestingly, for the HIT technology, the *k* value and, thus, the maximum power predicted by both models are very similar throughout the year, with only slight differences during summer and fall. In the case of the tandem technology, the FF_k model results in higher *k* values than Osterwald's, indicating that it simulates the power produced closer to the measured one, especially at the end of summer. Furthermore, for the tandem technology, the seasonal behavior of *k* is different than for the other technologies. Here, the *k*-value reaches its highest value during summer/fall.

This distinct seasonal behavior of the different technologies indicates that G_i and T_c may not be sufficient to correctly predict the power. Other parameters, which are not considered in the models, may also affect the predicted power depending on the season. These other parameters could be ambient parameters, such as the diffuse irradiance factor and/or the spectral distribution. The crystalline and thin-film silicon technologies may respond differently to these additional parameters due to their distinct low irradiance behavior, angular response and spectral response [10]. Further measurements of another year are needed to corroborate if the observed seasonal trends of their *k* values are periodic.

Some trends of the monthly *k* values can also be observed in the *k* values calculated for the entire year. For instance, for the Al-BSF technology, the annual *k* value obtained from Osterwald's model is higher than the one obtained from the FF_k model. For the HIT technology the *k* values of both models are almost the same. The tandem technology works better with the FF_k model, and its annual *k* values are the closest to 1 among the three technologies. This means the maximum power prediction of both models works most accurately for the tandem PV technology.

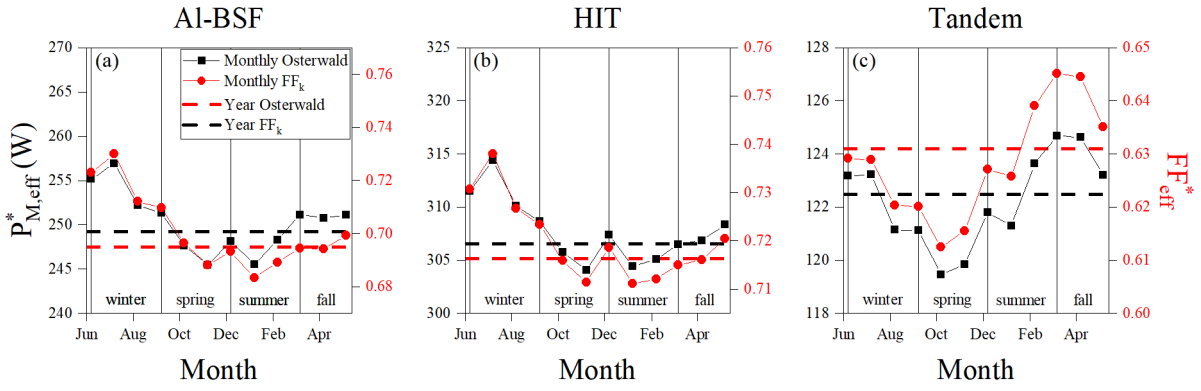

Figure 6. Effective parameters on a monthly and annual basis for both models for three technologies: (a) Al-BSF, (b) HIT, and (c) tandem.

Figure 6 shows the values of the effective parameters, $P^*_{M,eff}$ and FF^*_{eff}, which are calculated from *k* using equations (7) and (8). Hence, they demonstrate the same behavior and trends as observed for *k* in figure 5. It should be noted that the superior limits of the y-axis in figures 6 (a), (b) and (c) are the calibrated values from Table 1 as reference. This is to visualize the difference of the effective values to the calibrated ones nearest to STC. We can draw a similar conclusion for the effective parameters as for *k*: the behavior for each module could be attributed to the yearly average impact of other ambient parameters not considered in the models.

With the resulting effective parameters in figure 6, we can then recalculate the modeled power with equations (1) and (2), for each month and the entire year. To analyze the goodness of each method, the linear tendency was corroborated after the implementation of the correction factor.

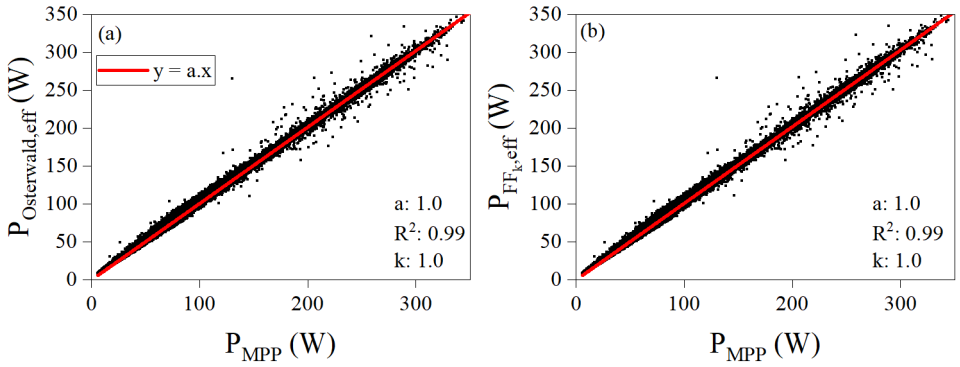

Figure 7. Correlation of the predicted and measured power using (a) Osterwald and (b) FF_k models after applying the correction factor k. Here, 1-year of data for the HIT module is analysed.

Figure 7 exemplarily shows the relation of the measured versus the "corrected" modeled power for the HIT technology using the data sets of the entire year. Now, due to the implementation of the correction factor, the resulting slope is a = 1.0 for both methods. The same behavior was observed for the all three technologies for data from each month and the entire year.

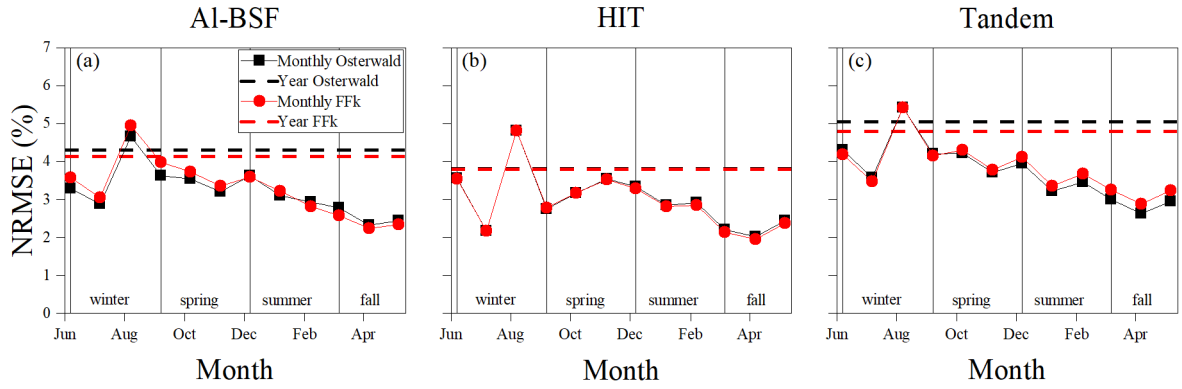

Figure 8. Normalized Root Mean Square Error (NRMSE) for each technology and model on a monthly, and annual basis for the three module technologies: (a) Al-BSF, (b) HIT, and (c) tandem.

Figure 8 depicts the resulting monthly and annual NRMSE values for each PV technology after the implementation of the correction factor. It is worth mentioning that for each month, a minimum of 2000 measurements were analyzed for each technology. Hence, the NRMSE value is based on sufficient data sets to have a reliable statistic to re-construct the error distribution, as suggested in [22]. In figure 8, both models result in very similar NRMSEs, and thus also dispersion, for any month and technology. However, for all three technologies, one can observe that the monthly NRMSE value has a maximum in the month of August and then decreases from spring to fall. It will be interesting to see if this behavior is periodic and repeats itself in the following years. The tandem technology shows the highest annual NRMSE value and the HIT the lowest. Further studies will aim at a better understanding of this behavior.

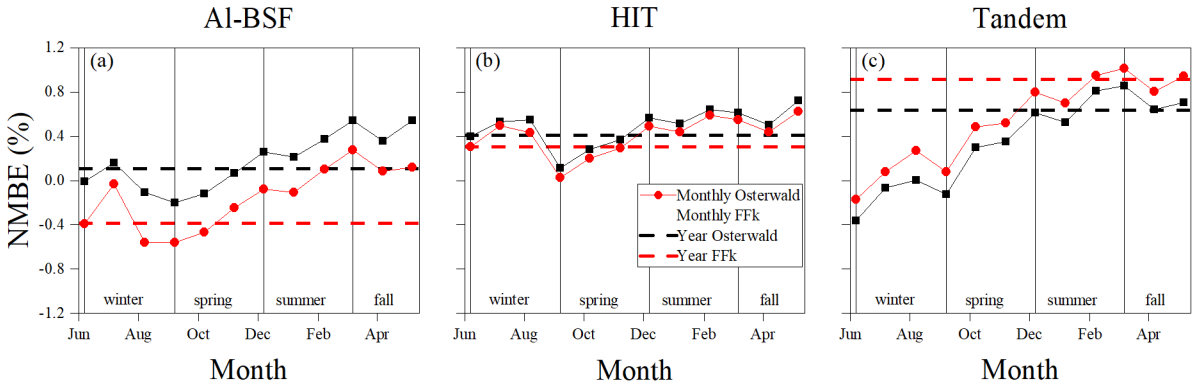

Figure 9. Normalized Mean Bias Error (NMBE) for each technology and model on a monthly and annual basis: (a) Al-BSF, (b) HIT and (c) tandem.

Figure 9 depicts the monthly and annual values of the NMBE for the three PV technologies. All NMBE values are relatively small, below 1%. This is expected since the purpose of the implementation of the correction factor was to minimize the NMBE. Nevertheless, despite the correction factor, a positive NMBE value indicates that the model is still overestimating, a negative value means it is underestimating the power. In the case of the Al-BSF, for Osterwald's model, the annual NMBE is closest to 0, which implies that the implementation of the correction factor seems to be most effective for this technology in maximizing the prediction accuracy. The FF_k model tends to underestimate the power. For the HIT technology, both models present similar, annual, positive NMBE values. These remain mostly stable during the entire year, slightly overestimating the modeled power with values ranging from about 0 to 0.8 %. For the tandem, both models tend to overestimate the measured power with a tendency to higher values over the months. Osterwald's method results in lower NMBE values than the FF_k method.
In Table 2, we summarize the annual values of the calculated parameters k, $P^*_{M,eff}$, FF^*_{eff}, NRMSE, and NMBE, each for both models and three technologies. For the Al-BSF technology, the correction factor closer to 1 implies that Osterwald's model better predicts the power than the FF_k model when using the calibrated parameters, i.e. without the correction factor k. Furthermore, for the Osterwald model, lower absolute values of NRMSE and NMBE, which are closer to 0, imply that this is also the case after applying the correction factor and using the effective parameters for the power prediction. Whereas for the HIT technology, there is no clear difference in using either model with or without k, since their k values as well as NRMSE and NMBE do not differ much. Finally, for the tandem technology, the FF_k method may be recommended if calibrated values are being used for power prediction, due to its slightly lower k value. However, Osterwald's model behaves slightly better if the correction factor is applied, as can be seen by the lower NRMSE and NMBE values.

Table 2. Annual values of k, $P^*_{M,eff}$, FF^*_{eff}, NRMSE, and NMBE; for Osterwald and FF_k for each technology (Al-BSF, HIT, and tandem).

Technology	Method	k	$P^*_{M,eff}$ (W)	FF^*_{eff}	$NRMSE$ (%)	$NMBE$ (%)
Al-BSF	Osterwald	0.93	249.20	-	3.50	0.11
	FF_k	0.90	-	0.69	3.63	-0.39
HIT	Osterwald	0.94	306.52	-	3.10	0.40
	FF_k	0.94	-	0.72	3.08	0.28
Tandem	Osterwald	0.96	122.47	-	4.13	0.64
	FF_k	0.97	-	0.63	4.46	0.91

5. Conclusions

In this work we carried out an experimental campaign of one year to monitor the power and compare two relatively simple models, Osterwald's and constant fill factor (FF_k) to predict the power of three PV technologies: Al-BSF, HIT and a-Si/µc-Si tandem. The power was monitored through I-V curve measurements. The models predicted the power based on measurements of the in-plane irradiance and the module temperature. Both models resulted in an overestimation of the estimated power by about 2 to 10% depending on the month and PV technology. To minimize the overestimation, a correction factor was introduced on a monthly and annual basis. The monthly values of the correction factor indicated different trends during the different seasons of the year. Furthermore, the trends differed also for the distinct PV technologies, particularly when comparing the crystalline based technologies, Al-BSF and HIT, with the a-Si/µc-Si tandem thin-film technology. This could be associated to variables besides the irradiance and module temperature, that the models do not consider, such as the spectral distribution and/or the diffuse irradiance factor. Further studies will need to be performed to understand this behavior.

By applying this correction factor to the models on an annual basis, the NMBE of the predicted maximum power was minimized for all technologies. NMBEs below 1% indicate a high accuracy in their prediction capability. Furthermore, NRMSEs below 5% indicate a low dispersion of the predicted values. A closer look, seeking technology-specific evaluations of the prediction capabilities of both models, indicate that: For the Al-BSF technology Osterwald's model can be recommended for estimating the power in any case with or without the implementation of the correction factor. In the case of HIT technology, no clear difference between the two models in their prediction accuracy, neither before nor after applying the correction factor. Finally, for the tandem technology, the FF_k model is recommended when using the calibration values, while Osterwald's model has a slightly higher accuracy after the implementation of the correction factor.

6. Acknowledgements

We acknowledge the financial support provided by the Peruvian National Fund for Scientific and Technological Development (FONDECYT) through Contract N° 124-2018-FONDECYT. Additional support was provided by the vice-chancellorship for research of the Pontificia Universidad Católica del Perú (PUCP) (project no. CAP-2019-3-0041/702). Brando Calsi received financial support by Bachelor Thesis Development Support Program (PADET).

7. References

[1] Espinoza R, Luque C and Casa J De 2016 Missing gaps in the challenge of massive intervention of grid-connected PV systems in Peru *European Photovoltaic Solar Energy Conference and Exhibition* pp 3048–52

[2] Feron S and Cordero R R 2018 Is Peru prepared for large-scale sustainable rural electrification? *Sustain.* **10** 1–20

[3] Zambrano-Monserrate M A, Silva-Zambrano C A, Davalos-Penafiel J L, Zambrano-Monserrate A and Ruano M A 2018 Testing environmental Kuznets curve hypothesis in Peru: The role of renewable electricity, petroleum and dry natural gas *Renew. Sustain. Energy Rev.* **82** 4170–8

[4] Romero-Fiances I, Muñoz-Cerón E, Espinoza-Paredes R, Nofuentes G and de la Casa J 2019 Analysis of the Performance of Various PV Module Technologies in Peru *Energies* **12** 186

[5] Moser D, Buono M Del, Jahn U, Herz M, Richter M and Brabandere K De 2017 Identification of technical risks in the photovoltaic value chain and quantification of the economic impact *Prog. Photovoltaics Res. Appl.* **25** 592–604

[6] International Electrotechnical Commission 2008 *Photovoltaic devices - Part 3: measurement principles for terrestrial photovoltaic (PV) solar devices with reference spectral irradiance data*

[7] Zaihidee F M, Mekhilef S, Seyedmahmoudian M and Horan B 2016 Dust as an unalterable deteriorative factor affecting PV panel's efficiency: Why and how *Renew. Sustain. Energy*

Rev. **65** 1267–78
[8] Afonso M M D, Carvalho P C M, Antunes F L M and Hiluy Filho J J 2017 Deterioration and performance evaluation of photovoltaic modules in a semi-arid climate *Renew. Energy Power Qual. J.* 424–8
[9] Torres-Ramírez M, Nofuentes G, Silva J P, Silvestre S and Muñoz J V. 2014 Study on analytical modelling approaches to the performance of thin film PV modules in sunny inland climates *Energy* **73** 731–40
[10] Schweiger M, Herrmann W, Gerber A and Rau U 2017 Understanding the energy yield of photovoltaic modules in different climates by linear performance loss analysis of the module performance ratio *IET Renew. Power Gener.* **11** 558–65
[11] Rus-Casas C, Aguilar J D, Rodrigo P, Almonacid F and Pérez-Higueras P J 2014 Classification of methods for annual energy harvesting calculations of photovoltaic generators *Energy Convers. Manag.* **78** 527–36
[12] Fuentes Conde M 2009 *Contribución al modelado del comportamiento eléctrico a sol real de módulos fotovoltaicos de silicio cristalino y CIS* (Universidad de Jaén)
[13] Conde L A, Montes-Romero J, Carhuavilca A, Perich R, Guerra J A, Sevillano M, Calsi B X, Angulo J R, De la Casa J and Töfflinger J A 2020 Implementation of a laboratory for the outdoor characterization of photovoltaic technologies under the climatic conditions of Lima *Tecnia* vol 30 pp 80–9
[14] Conde L A, Montes-Romero J, Carhuavilca A, Perich R, Jorge A, Angulo J, Muñoz E, Töfflinger J A and Casa J De 2020 Performance evaluation and characterization of different photovoltaic technologies under the coastal , desertic climate conditions of Lima , Peru *Solar World Congress* p 11
[15] Montes-Romero J, Piliougine M, Muñoz J V, Fernández E F and De La Casa J 2017 Photovoltaic device performance evaluation using an open-hardware system and standard calibrated laboratory instruments *Energies* **10** 1869
[16] Ishii T, Otani K and Takashima T 2011 Effects of solar spectrum and module temperature on outdoor performance of photovoltaic modules in round-robin measurements in Japan *Prog. Photovoltaics Res. Appl.* **19** 141–8
[17] D'Orazio M, Di Perna C and Di Giuseppe E 2014 Experimental operating cell temperature assessment of BIPV with different installation configurations on roofs under Mediterranean climate *Renew. Energy* **68** 378–96
[18] Silva J S, Rojas J P, Norabuena M and Seguel R J 2018 Ozone and volatile organic compounds in the metropolitan area of Lima-Callao, Peru *Air Qual. Atmos. Heal.* **11** 993–1008
[19] Fuentes M, Nofuentes G, Aguilera J, Talavera D L and Castro M 2007 Application and validation of algebraic methods to predict the behaviour of crystalline silicon PV modules in Mediterranean climates *Sol. Energy* **81** 1396–408
[20] Osterwald C R 1986 Translation of device performance measurements to reference conditions *Sol. Cells* **18** 269–79
[21] Ramon Ruiz G and Fernández Bandera C 2017 Validation of Calibrated Energy Models: Common Errors *Energies* **10** 19
[22] Chai T and Draxler R R 2014 Root mean square error (RMSE) or mean absolute error (MAE)? - Arguments against avoiding RMSE in the literature *Geosci. Model Dev.* **7** 1247–50